Renormalization group study of intervalley scattering and valley splitting in a two-valley system

Alexander Punnoose*
Physics Department, City College of the City University of New York, New York, New York 10031, USA
(Received 30 September 2009; revised manuscript received 17 November 2009; published 7 January 2010)

Renormalization group equations are derived for the case when both valley splitting and intervalley scattering are present in a two-valley system. A third scaling parameter is shown to be relevant when the two bands are split but otherwise distinct. The existence of this parameter changes the quantitative behavior at finite temperatures, but the qualitative conclusions of the two-parameter theory are shown to be unaffected for realistic choice of parameters.

DOI: 10.1103/PhysRevB.81.035306 PACS number(s): 72.10.−d, 71.30.+h, 71.10.Ay

I. INTRODUCTION

Renormalization group (RG) studies of multivalley two-dimensional electron gas (2DEG) systems have been very successful in quantitatively describing the transport properties of electrons confined in silicon inversion layers [metal-oxide-semiconductor field-effect transistors (MOSFETs)].[1–5] In a disordered medium, for temperatures $k_BT<\hbar/\tau$, where $1/\tau$ is the elastic scattering rate, the propagating modes are diffusive, and it is now well understood that these modes play a central role in determining the transport properties at low temperatures.[6] In two dimensions, in particular, the effects of diffusion are profound. The electron-electron (e-e) scattering amplitudes, for example, develop nonanalytic corrections that result in enhanced correlations at low energies.[7] It has been shown that RG theory applied to a weakly disordered system is able to capture this scale (energy or temperature) dependence to all orders in the e-e scattering amplitudes making it the most promising analytical technique available to understand the physics of disordered systems. (Pedagogical reviews of the RG theory can be found in Refs. 8 and 9.)

Weak disorder implies that $\hbar/\tau<E_F$, where E_F is the Fermi energy. Typical high-mobility two-dimensional semiconducting devices have very small Fermi energies with a scattering rate which is even smaller due to the very high mobility of the samples making it very difficult to access the diffusive region at experimentally reasonable temperatures. Si-MOSFETs, on the other hand, have only moderately high mobilities so that $\hbar/\tau$ is of the order of a kelvin while E_F is of the order of a few kelvin. The impurity scattering in these inversion layers is short ranged in character making quantum scattering the dominant scattering mechanism, while semiclassical effects arising from the impurity potential landscape are negligible at low temperatures. For these reasons, as noted in the beginning, RG theory has been particularly successful in describing the properties of electrons in silicon inversion layers. (See Ref. 3 for how the diffusive regime is identified experimentally and for a quantitative comparison of theory with experiment.)

The conduction band of an n-(001) silicon inversion layer has two almost degenerate valleys located close to the X points in the Brillouin zone.[10] The abrupt change in the potential at the interface, which breaks the symmetry in the z direction perpendicular to the 2D plane, leads to the splitting of the two valleys. Although intervalley scattering originates from both impurity scattering and scattering due to e-e interactions, the imperfections at the interface, which are distributed on the atomic scale, are the main source of the large momentum transfer Q_0 in the z direction needed for intervalley scattering.

The RG theory developed in Ref. 1 considered the valley degrees of freedom to be degenerate and distinct; hence, quantitative comparisons with experiments performed in Ref. 3 were limited to temperatures larger than the valley splitting, Δ_v, and the intervalley scattering rate, $\hbar/\tau_\perp$, both scales being sample dependent. This paper develops the relevant scaling equations in the presence of valley splitting and intervalley scattering. When combined with the scaling equations in a parallel magnetic field in the presence of valley splitting developed in Ref. 11, they provide a complete description of the low-temperature transport properties of MOSFETs. It should be noted that the RG theory is developed to first order in the resistance (one-loop) and hence is applicable only in the metallic phase not too close to the observed metal-insulator transition.[12] Also, since it is seen experimentally that the phase breaking rate saturates at low temperatures for low electron densities,[13] where the results obtained in this paper are most relevant, the contribution from the cooperon (particle-particle) channel has been suppressed in our calculations.

The scaling equations are presented in three different temperature regimes: (i) high-temperature region, $T\gtrsim T_v$ and $T_\perp$, where $k_BT_v=\Delta_v$ and $k_BT_\perp=\hbar/\tau_\perp$, (ii) low-temperature region, $T\lesssim T_\perp$, (iii) and intermediate temperature region, $T_\perp \lesssim T\lesssim T_v$. The last of the three regions is relevant when the band splitting is large so that effective mixing of the valleys due to impurity scattering occurs only at sufficiently low temperatures; it is shown that the standard two-parameter description has to be modified in this case to include a third scaling variable which has quantitative effects at finite temperature but does not affect the asymptotic conclusions of the two-parameter theory. The interaction in the Cooperon channel has been suppressed in these calculations.

II. DIFFUSION MODES AND FERMI-LIQUID AMPLITUDES

Electrons in valleys can be conveniently labeled using additional valley indices $\tau_z=\pm$. (For our purpose, the num-

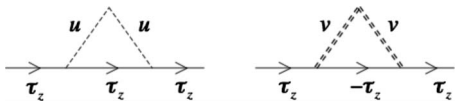

FIG. 1. Diagrams contributing to $1/\tau$ in Eq. (2) are shown. The properties of the intravalley and intervalley impurity scatterings are defined in Eq. (1) represented here by single and double dashed lines, respectively.

ber of valleys $n_v=2$ located at $\pm Q_0\hat{z}$, where $Q_0 \approx 0.85 \times (2\pi/a)$ with a being the lattice constant of silicon.) This increases the number of single-particle states to (spin) $\times$(valley)=4. Since the diffusion modes, responsible for the relaxation of density and spin perturbations (and valley in our case) in a disordered system at long times and distances, formally occur via particle-hole excitations, the corresponding number of (particle) $\otimes$ (hole) diffusion modes equals 16. This is a fourfold increase from the case of one valley and has significant quantitative effects on transport as shown in Ref. 1. At low temperatures, some of these modes develop gaps (cutoffs) proportional to Δ_v and $\hbar/\tau_\perp$ and are therefore ineffective (nonsingular) for T below the characteristic temperature scales T_v and $T_\perp$,[14,15] leading to quantitatively different scaling as the temperature is varied.

A. Single-particle properties

At low electron densities the mobility of a 2DEG is determined by the charged centers within the SiO_2 layer. Due to the short-ranged nature of the impurity scattering in silicon inversion layer structures, the Drude relation for the mobility, $\mu=e\tau/m$, gives a direct measure of the single-particle lifetime, τ. Here, e and m are the charge and the effective mass of the electron, respectively. Ando[16] argued that the mobility is also determined partially by the intervalley scattering rate. To this end, the two different scattering rates, that is, the intravalley and intervalley rates, can be incorporated by introducing two scattering potentials,[15] $u(\mathbf{q})$ and $v(\mathbf{q})$, respectively. The potential $u(\mathbf{q})$ is slowly varying on the scale of $1/a$ if the impurities in the oxide layer is uniformly distributed, while $v(\mathbf{q})$ is a rapidly oscillating function with momentum of the order of $1/a$. Hence, the random average of the potentials $\langle u(\mathbf{q})v(\mathbf{q})\rangle=0$, with $u(\mathbf{q})$ and $v(\mathbf{q})$ satisfying

$$\langle u(\mathbf{q})u(\mathbf{q}')\rangle = \delta_{\mathbf{q}+\mathbf{q}'}\frac{1}{2\pi\nu\tau_\parallel}, \tag{1a}$$

$$\langle v(\mathbf{q})v(\mathbf{q}')\rangle = \delta_{\mathbf{q}+\mathbf{q}'}\frac{1}{2\pi\nu\tau_\perp}, \tag{1b}$$

where $\nu=m/2\pi$ is the density of states per spin and valley. The total lifetime, τ, then equals (see Fig. 1)

$$\frac{1}{\tau} = \frac{1}{\tau_\parallel} + \frac{1}{\tau_\perp}. \tag{2}$$

B. Particle-hole diffusion propagators

The form of the particle-hole propagators (diffusons) for the impurity model defined in Eq. (1) has been calculated in Refs. 14 and 15. The calculations are extended here to include valley splitting.

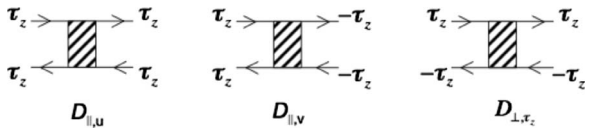

FIG. 2. The various diffuson blocks in the presence of valley splitting and intervalley scattering are shown.

The fluctuations in the diffuson channel, $\mathcal{D}(q,\omega)$, have a diffusive singularity $\mathcal{D}(q,\omega)=1/(D_0q^2+|\omega|)$. Finite valley splitting and intervalley scattering introduce gaps in $\mathcal{D}(q,\omega)$, thus, cutting off the singularity. The different diffuson modes involving fluctuations in the valley occupations are shown in Fig. 2. The details of their derivation are given in Appendix A.

We start by defining the elementary diffuson blocks, $\mathcal{D}_{\parallel,u}$, $\mathcal{D}_{\parallel,v}$, and $\mathcal{D}_{\perp,\tau_z}$ shown in Fig. 2. The diffuson blocks $\mathcal{D}_\parallel$ are insensitive to valley splitting since both the particle and the hole (corresponding to the top and bottom lines with arrows moving to the right and left, respectively) belong to the same valley. The τ_z index for the $\mathcal{D}_{\perp,\tau_z}$ diffuson indicates the valley index of the particle, with the hole being in the $-\tau_z$ valley; the two valleys are nonequivalent for finite Δ_v. In Appendix A, the equations satisfied by the diffuson propagators are solved in the limit of weak splitting $\Delta_v\tau \lesssim 1$. The solutions are expressed in terms of the diffusons $\mathcal{D}_\pm = \mathcal{D}_{\parallel,u} \pm \mathcal{D}_{\parallel,v}$ and $\mathcal{D}_{\perp,\tau_z}$, with the corresponding gaps $\Delta_- = 2\tau_\parallel/\tau(\tau_\perp-\tau_\parallel)$ and $\Delta_\perp=\tau_\parallel/\tau\tau_\perp$. (Note that $\mathcal{D}_+$, corresponding to the valley "singlet" mode, is gapless, hence, $\Delta_+=0$.)

In the limit when the intervalley scattering is much weaker than the intravalley scattering, i.e., $\tau_\perp \gg \tau_\parallel$, the scattering time $\tau \approx \tau_\parallel$. The gaps in this limit correspond to $\Delta_- \approx 2/\tau_\perp$ and $\Delta_\perp \approx 1/\tau_\perp$. In this weak scattering limit, relevant to high-mobility MOSFETs, the form of the diffusons obtained in Eqs. (A3) and (A4) reduces to (the overall factor $1/2\pi\nu\tau^2$ is suppressed)

$$\mathcal{D}_+(q,\omega) = \frac{1}{D_0q^2+|\omega|}, \tag{3a}$$

$$\mathcal{D}_-(q,\omega) = \frac{1}{D_0q^2+|\omega|+2\Delta_\perp}, \tag{3b}$$

$$\mathcal{D}_{\perp,\tau_z}(q,\omega) = \frac{1}{D_0q^2+|\omega|-i\tau_z\Delta_v+\Delta_\perp}, \tag{3c}$$

where $\Delta_\perp=1/\tau_\perp$. The number of modes that are effectively gapless depends on the relative magnitude of T (or frequency) with respect to the corresponding temperature scales T_v and $T_\perp$. At high-T all modes are gapless, while at the lowest T only $\mathcal{D}_+$ remains gapless. [Note that the valley splitting term in Eq. (3c) is similar in structure to Zeeman splitting.[17]]

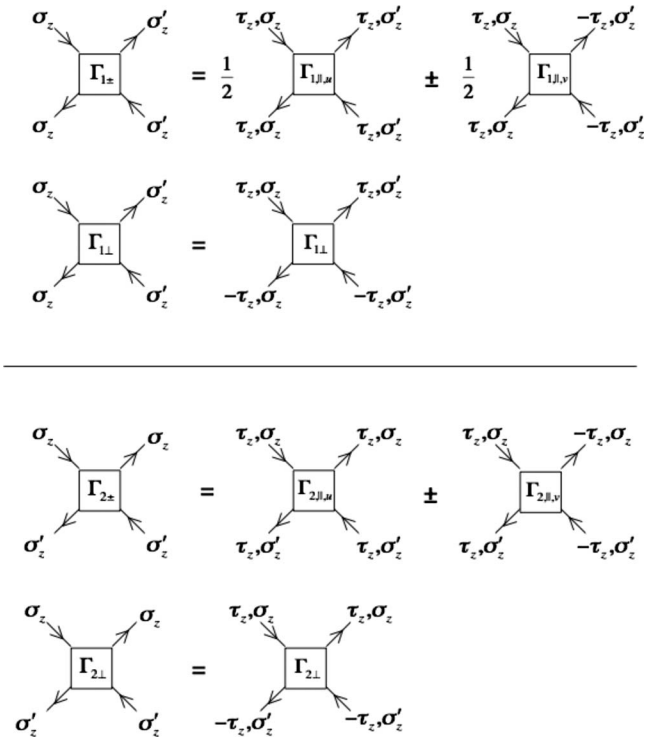

FIG. 3. The scattering amplitudes including the valley degrees of freedom are classified in terms of the standard static Fermi-liquid amplitudes Γ_1 and Γ_2. The same subscript convention used to classify the diffusons in Fig. 2 is used here.

C. Electron-electron scattering amplitudes

In this section the relevant *e-e* interaction scattering amplitudes are identified. These amplitudes are conventionally described by the standard static Fermi-liquid amplitudes Γ_1 and Γ_2 defined in terms of the spin texture of the scattering of the particle-hole pairs. The amplitudes are easily generalized to include the valley degrees of freedom. They are shown in Fig. 3. Note that the intervalley scattering amplitudes $\Gamma_{1\perp}$ and $\Gamma_{2,\parallel,v}$ are generally negligibly small in a clean system because the Coulomb scattering involving large momentum Q_0 in the z direction is suppressed when the width of the inversion layer is many times larger than the lattice spacing. It is more convenient to work in the same basis as that used for the diffusons, i.e., $\Gamma_{1\pm}=\frac{1}{2}(\Gamma_{1,\parallel,u}\pm\Gamma_{1,\parallel,v})$ and $\Gamma_{2\pm}=(\Gamma_{2,\parallel,u}\pm\Gamma_{2,\parallel,v})$, as it allows for the amplitudes to be easily combined with the diffusion modes.

III. DIFFUSION CORRECTIONS

It is now well understood that while the diffusion propagators when combined with *e-e* scattering lead to the appearance of logarithmic corrections to the resistivity (Altshuler-Aronov corrections[6,18]), the *e-e* scattering amplitudes themselves develop logarithmic corrections due to the slow diffusive relaxation.[7] In this section, these logarithmic corrections are obtained self-consistently in the limit of weak valley splitting ($\Delta_v\tau\lesssim 1$) and weak intervalley scattering ($\tau_\perp \gg \tau_\parallel$).

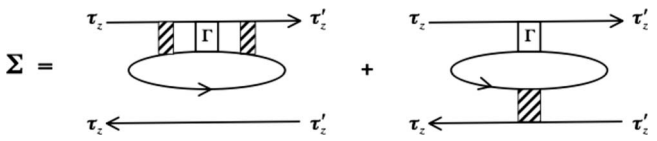

FIG. 4. The skeleton diagrams for Σ are listed. Γ is the interaction matrix and the hashed blocks are diffusion propagators. The Σ_+ matrix is obtained by adding the contributions from $\tau_z'=\pm\tau_z$. The results are presented in Eq. (B1).

The *e-e* interaction corrections to the diffusion propagators are expressed in terms of the "self-energy" matrix Σ. The relevant diagrams are shown in Fig. 4. Expanding $\Sigma(q,\omega)$ to order q^2 and ω one obtains, for example, for the gapless $\mathcal{D}_+$ propagator, the renormalized propagator $\mathcal{D}_+^{-1}(q,\omega)=Dq^2+z\omega$, where D is the renormalized diffusion constant and z is the frequency renormalization parameter that determines the change in the relative scaling of the frequency with respect to the length scale[7,19] ($z=1$ for noninteracting electrons). The corresponding corrections to D and z obtained by evaluating the diagrams in Fig. 4 are given in Eq. (B1) in Appendix B.

The skeleton diagrams representing the diffusion corrections to the *e-e* scattering amplitudes are shown in Fig. 5. (For a detailed discussion of these corrections, see Refs. 8 and 9.) The calculations are generalized here to include valleys. By appropriately choosing the Γ vertices for given values of $\tau_z'=\pm\tau_z$ in Fig. 5 all the corrections, $\delta\Gamma_{i,\alpha}$, to the scattering amplitudes $\Gamma_{i,\alpha}$, where $i=1,2$ and $\alpha=\pm$, can be calculated. For example, to calculate $\delta\Gamma_{i+}$, since $\Gamma_{i+}=\Gamma_{i,\parallel,u}+\Gamma_{i,\parallel,v}$, the contributions from $\tau_z'=\pm\tau_z$ are added, while they are subtracted when calculating $\delta\Gamma_{i-}$. The results are given in Eq. (B2) in Appendix B. (The corrections to the amplitude $\delta\Gamma_\perp$ are not given as they are equal to $\delta\Gamma_{2+}$ for $T\gtrsim T_v$ and irrelevant for $T\lesssim T_v$ due to the gap.)

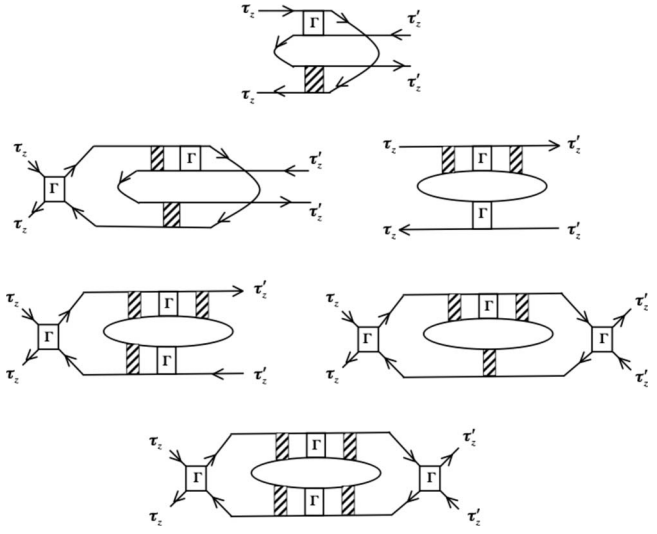

FIG. 5. Skeleton diagrams for $\delta\Gamma_{i,\alpha}$. By appropriately choosing the Γ vertices for given values of $\tau_z'=\pm\tau_z$ all the corrections $\delta\Gamma_{i,\alpha}$, where $i=1,2$ and $\alpha=\pm$, are calculated. Each combination of the valley indices comes together with the appropriate diffuson matrix elements. Note that going down the rows increases the number of Γ vertices.

The corrections δD, δz, and $\delta\Gamma_{i,\alpha}$ in Eqs. (B1) and (B2) include all modes, both gapped and gapless. Clearly, only modes that are effectively gapless lead to logarithmically divergent corrections. Since the frequency integrations range from $T \lesssim \omega \lesssim 1/\tau$ (the upper cutoff follows from taking the diffusion limit), for $T \lesssim T_\perp$, both $\mathcal{D}_-$ and $\mathcal{D}_\perp$ are gapped, while only the $\mathcal{D}_-$ modes are effectively gapless when $T_\perp \lesssim T \lesssim T_v$. (The $\mathcal{D}_+$ mode is always gapless.) Of course, when $T \gtrsim T_v$ and $T_\perp$, all modes are gapless. As a result, the corrections are clearly sensitive to the temperature range considered.

A. High-temperature range: $T \gtrsim T_v$ and $T_\perp$

For $T \gtrsim T_v$ and $T_\perp$, all the modes $\mathcal{D}_\alpha$ ($\alpha = \pm, \perp$) appearing in Eqs. (B1) and (B2) are effectively gapless; i.e., they take the form $\mathcal{D}(q,\omega) = 1/(Dq^2 + z\omega)$. As noted below, not all amplitudes $\Gamma_{i,\alpha}$ are relevant at these temperatures. For instance, since intervalley scattering is irrelevant for $T \gtrsim T_\perp$, the amplitudes $\Gamma_{1\perp}$ and $\Gamma_{2,\parallel,v}$, whose initial values are vanishingly small, can be set to zero. As a result (see Fig. 5), $\Gamma_{1\perp} \approx 0$ and $\Gamma_{2+} \approx \Gamma_{2-}$. Furthermore, since valley splitting can be ignored for $T \gtrsim T_v$, the amplitudes $\Gamma_{1,\parallel,u}$ and $\Gamma_{2\perp}$ are indistinguishable from the amplitudes $\Gamma_{1,\parallel,v}$ and Γ_{2+}, respectively, implying that the initial value of $\Gamma_{1-} = 0$ and $\Gamma_{2\perp} = \Gamma_{2+}$.

It can be seen from Eq. (B2) that choosing the above initial conditions, namely, $\Gamma_{1\perp} = \Gamma_{1-} = 0$, and setting all the $\Gamma_{2\alpha}$ amplitudes to be equal, and all the $\mathcal{D}_\alpha$ propagators to be gapless, gives $\delta\Gamma_{1-} = 0$ and $\delta\Gamma_{2-} = \delta\Gamma_{2+}$, which are consistent with the choice of the initial conditions. Hence, Eqs. (B1) and (B2) reduce to the form (with the substitution $\Gamma_{2\alpha} \equiv \Gamma_2$ and $\mathcal{D}_\alpha \equiv \mathcal{D}$)

$$\frac{\delta D}{D} = -\frac{4}{\nu}\int\int \frac{d\omega}{2\pi}(\Gamma_{1+} - 4\Gamma_2)\mathcal{D}^3(q,\omega)Dq^2, \tag{4a}$$

$$\delta z = -\frac{1}{\pi\nu}\int \frac{d^2q}{(2\pi)^2}(\Gamma_{1+} - 4\Gamma_2)\mathcal{D}(q,0), \tag{4b}$$

$$\delta\Gamma_{1+} = \frac{1}{\pi\nu}\int \frac{d^2q}{(2\pi)^2}\Gamma_2\mathcal{D}(q,0) + 4\Psi(\Gamma_2), \tag{4c}$$

$$\delta\Gamma_2 = \frac{1}{\pi\nu}\int \frac{d^2q}{(2\pi)^2}\Gamma_{1+}\mathcal{D}(q,0) + 16\Psi(\Gamma_2), \tag{4d}$$

where $\int\int = \int d^2q/(2\pi)^2 \int d\omega/(2\pi)$ and $\Psi(\Gamma_2)$ equals

$$\begin{aligned}\Psi(\Gamma_2) = &+\frac{1}{\nu}\int \frac{d^2q}{(2\pi)^2}\int \frac{d\omega}{2\pi}\Gamma_2[\Gamma_2\mathcal{D}^2] - \frac{1}{2}[\Gamma_2^2\mathcal{D}^2] \\ &- \frac{1}{\nu}\int \frac{d^2q}{(2\pi)^2}\int \frac{d\omega}{2\pi}\omega\Gamma_2[\Gamma_2^2\mathcal{D}^3] - \omega\Gamma_2^2[\Gamma_2\mathcal{D}^3] \\ &- \frac{2}{\nu}\int \frac{d^2q}{(2\pi)^2}\int \frac{d\omega}{2\pi}\omega^2\Gamma_2^2[\Gamma_2^2\mathcal{D}^4].\end{aligned} \tag{5}$$

The above equations were first obtained in Ref. 1; they correspond to the case when the two valleys are distinct and degenerate.

B. Low-temperature range: $T \lesssim T_\perp$

When $T \lesssim T_\perp$, both $\mathcal{D}_-$ and $\mathcal{D}_\perp$ are gapped and therefore irrelevant. Hence, only the $\mathcal{D}_+$ mode survives. Dropping the contributions of the gapped modes in Eqs. (B1) and (B2) lead to a self-contained set of equations involving only the amplitudes $\delta\Gamma_{1+}$ and $\delta\Gamma_{2+}$. The equations, after dropping the + sign in $\mathcal{D}_+$ and Γ_{2+}, reduce to

$$\frac{\delta D}{D} = -\frac{4}{\nu}\int\int (\Gamma_{1+} - \Gamma_2)\mathcal{D}^3(q,\omega)Dq^2, \tag{6a}$$

$$\delta z = -\frac{1}{\pi\nu}\int \frac{d^2q}{(2\pi)^2}(\Gamma_{1+} - \Gamma_2)\mathcal{D}(q,0), \tag{6b}$$

$$\delta\Gamma_{1+} = \frac{1}{4\pi\nu}\int \frac{d^2q}{(2\pi)^2}\Gamma_2\mathcal{D}(q,0) + \Psi(\Gamma_2), \tag{6c}$$

$$\delta\Gamma_2 = \frac{1}{\pi\nu}\int \frac{d^2q}{(2\pi)^2}\Gamma_{1+}\mathcal{D}(q,0) + 4\Psi(\Gamma_2). \tag{6d}$$

These equations correspond to the case when the two valleys appear as a single valley due to intervalley scattering. (Note that valley splitting is irrelevant in this case as the $\mathcal{D}_\perp$ propagator is always gapped when $T \lesssim T_\perp$ irrespective of T_v.)

C. Intermediate temperature range: $T_\perp \lesssim T \lesssim T_v$

This limit when the valley splitting is large, so that the intervalley scattering rate $T_\perp \ll T_v$, is interesting. For temperatures in the intermediate range $T_\perp \lesssim T \lesssim T_v$, only the $\mathcal{D}_\perp$ mode is gapped, while both $\mathcal{D}_\pm$ are gapless. Although the initial value of $\Gamma_{1-} \approx 0$ when $T \gtrsim T_v$ (see discussion in Sec. III A) it can be seen from Eq. (B2) that $\delta\Gamma_{1-} \neq 0$ when $T \lesssim T_v$ and is therefore generated at intermediate temperatures. This introduces a third relevant scaling parameter distinct from the high- and low-temperature regimes. (Since $T \gtrsim T_\perp$, $\Gamma_{2+} = \Gamma_{2-}$, but because $T \lesssim T_v$ the $\Gamma_{2\perp}$ amplitude is irrelevant.)

Dropping the $\mathcal{D}_\perp$ terms in Eqs. (B1) and (B2) and setting $\Gamma_{2+} = \Gamma_{2-} \equiv \Gamma_2$ and $\mathcal{D}_\pm = \mathcal{D}$ give

$$\frac{\delta D}{D} = -\frac{4}{\nu}\int\int (\Gamma_{1-} + \Gamma_{1+} - 2\Gamma_2)\mathcal{D}^3(q,\omega)Dq^2, \tag{7a}$$

$$\delta z = -\frac{1}{\pi\nu}\int \frac{d^2q}{(2\pi)^2}(\Gamma_{1-} + \Gamma_{1+} - 2\Gamma_2)\mathcal{D}(q,0), \tag{7b}$$

$$\delta\Gamma_{1+} = \delta\Gamma_{1-} = \frac{1}{2\pi\nu}\int \frac{d^2q}{(2\pi)^2}\Gamma_2\mathcal{D}(q,0) + 2\Psi(\Gamma_2), \tag{7c}$$

$$\delta\Gamma_2 = \frac{1}{\pi\nu}\int \frac{d^2q}{(2\pi)^2}(\Gamma_{1+} + \Gamma_{1-})\mathcal{D}(q,0) + 8\Psi(\Gamma_2). \tag{7d}$$

Note that although both $\delta\Gamma_{1+}$ and $\delta\Gamma_{1-}$ are equal, their initial values are different.

The relevance of the Γ_{1-} amplitude in the temperature range $T_\perp \lesssim T \lesssim T_v$ is specific to problems with split bands

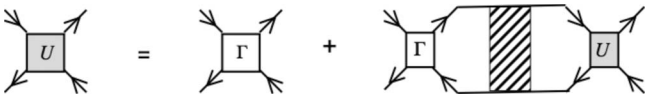

FIG. 6. Extending the static amplitudes Γ by the corresponding dynamic amplitudes U through ladder summations.

and was first discussed in Ref. 11 for the case of spin-splitting in a multivalley system.

IV. RENORMALIZATION GROUP EQUATIONS

In Sec. III, the leading logarithmic corrections in all the different temperature ranges have been listed. It is now possible to set up the scaling equations. To this end, first note that all the corrections involve only one momentum integration, and since every momentum integration generates a factor of $1/D$, which by Einstein's relation is proportional to the resistance ρ, the corrections are limited to the first order in resistance (disorder). The limitation on the number of momentum integrations also constrains the number of e-e vertices in the skeleton diagrams shown in Figs. 4 and 5. These corrections can now be extended to all orders in Γ (but still first order in ρ) by performing ladder summations as shown in Fig. 6. It amounts to replacing the static amplitudes Γ by the dynamical amplitudes $U(q,\omega)$ as discussed below.

Since the ladder summations do not introduce additional momentum integrations, the resummation allows the corrections to be evaluated to infinite order in the interaction amplitude leaving ρ as the only expansion parameter in the theory.[7]

For the amplitudes $\Gamma_{2\alpha}$, the ladder sums are most easily done in the basis $\alpha=\pm$ and $\perp$, as it can be checked by inspection that the indices are conserved in the ladder. Using $\Gamma_{2\alpha}$ and $\mathcal{D}_\alpha$ in Fig. 6, one obtains the corresponding dynamical amplitude $U_{2\alpha}(q,\omega)$, where

$$U_{2\alpha}(q,\omega)=\Gamma_{2\alpha}\frac{\mathcal{D}_{2\alpha}(q,\omega)}{\mathcal{D}_\alpha(q,\omega)}. \tag{8}$$

The propagators $\mathcal{D}_\alpha$ are defined in Eq. (3) and

$$\mathcal{D}_{2\alpha}(q,\omega)=\frac{1}{Dq^2+(z+\Gamma_{2\alpha})\omega+\Delta_\alpha}. \tag{9}$$

It should be noted in, for example, Fig. 5, that only those interaction vertices involving frequency integrations can be extended to include dynamical effects. For convenience, the corresponding Γ_2 vertices are enclosed in square brackets in the function Ψ in Eq. (5). Substituting for Γ_2 in Eq. (5) with U_2 from Eq. (8) [the α index is dropped since only gapless modes have been retained in Eq. (5)] and performing the q and ω integrals lead to the very simple expression[7,9]

$$\Psi(\Gamma_2)=\left(\frac{\Gamma_2^2}{z}\right)\frac{\rho}{2}\log\left(\frac{1}{T\tau}\right). \tag{10}$$

The dimensional resistance $\rho=1/4(2\pi^2\nu D)$ corresponds to $(e^2/\pi h)R_\square$, where $R_\square$ is the sheet resistance. The factor 4 arises due to the spin and valley degrees of freedom and ν is the density of states per spin and valley. Also note that up to logarithmic accuracy the upper cutoff can be replaced with $1/\tau$. Since the remaining integrals in Eqs. (4a)–(4d), (5), (6a)–(6d), and (7a)–(7d) are of the form $\int d^2q\mathcal{D}(q,0)$, they can be evaluated directly as

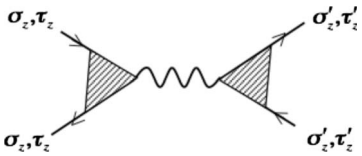

FIG. 7. The statically screened long-range part of the Coulomb interaction, which can be separated by cutting just one Coulomb line, is shown. The amplitude Γ_{0+} is obtained by adding the amplitudes with $\tau_z'=\pm$. The shaded triangles represent the static vertex corrections V.

$$\frac{1}{\pi\nu}\int\frac{d^2q}{(2\pi)^2}\mathcal{D}(q,0)=2\rho\log\left(\frac{1}{T\tau}\right). \tag{11}$$

It remains to evaluate the integrals for δD and δz. The δz integrals do not involve frequency integrations and can therefore be evaluated using Eq. (11). The δD corrections, however, contain frequency integrals, and therefore the $\Gamma_{1\pm}$ amplitudes, in addition to Γ_2, are also to be extended to all orders via the ladder sum.

This is most easily done in the spin-singlet basis

$$\Gamma_{s\pm}=\Gamma_{1\pm}-\frac{1}{4}\Gamma_{2\pm}. \tag{12}$$

This is so, because the spin and valley of the electron-hole pairs in the singlet and triplet basis are individually conserved in the ladder sum. (Note that the "+" amplitude is written in the (spin-singlet) ⊗ (valley-singlet) basis, while the "−" amplitude is in the (spin-singlet) ⊗ (valley-triplet) basis; the valley-triplet corresponds to $|S=1,\ S_z=0\rangle$.) The corresponding dynamical amplitudes $U_{s\pm}(q,\omega)$ on performing the ladder sum give

$$U_{s\pm}(q,\omega)=\Gamma_{s\pm}\frac{\mathcal{D}_{s\pm}(q,\omega)}{\mathcal{D}_\pm(q,\omega)}, \tag{13}$$

where

$$\mathcal{D}_{s\pm}(q,\omega)=\frac{1}{Dq^2+(z-4\Gamma_{s\pm})\omega+\Delta_\pm}. \tag{14}$$

(Note that Δ_+ is introduced for notational uniformity; in fact $\Delta_+=0$.)

Special attention is to be paid to the ladder sums involving Γ_{s+} when Coulomb interactions are present. The Γ_{1+} amplitudes in this case include amplitudes of the kind shown in Fig. 7, which can be separated by cutting the statically screened long-ranged Coulomb line once. They are denoted here as Γ_{0+}. This distinction is important because the polarization operator, $\Pi(q,\omega)$, which is irreducible to cutting a Coulomb line does not include Γ_{0+}. (The corresponding Γ_{0-} and $\Gamma_{0\perp}$ amplitudes are zero. The former is identically zero, while the latter involving intervalley scattering is vanishingly small.)

Analyzing the polarization operator, $\Pi(q,\omega)$, provides key insights into the relationship between the various amplitudes (and z).[8,9] The form of $\Pi(q,\omega)$ is analyzed here in the presence of valleys. In the limit of $q,\omega \to 0$, it can be shown that $\Pi(q,\omega)$ takes the form

$$\Pi(q,\omega) = -\frac{\partial n}{\partial \mu} + \frac{4V^2\omega}{Dq^2 + (z - 4\Gamma_{s+})\omega}. \tag{15}$$

It is important to note that only the Γ_{s+} amplitude, corresponding to the singlet mode, appears in the expression for $\Pi(q,\omega)$. The factor $\partial n/\partial \mu$ is the thermodynamic density of states and the parameter V is the static vertex corrections represented as shaded triangles in Fig. 7.

The two terms in Eq. (15) correspond to the static and the dynamical contributions, respectively. By construction, the static limit $\Pi(q \to 0, \omega = 0) = -\partial n/\partial \mu$ is satisfied. In the opposite limit, local conservation law requires that $\Pi(q=0, \omega \to 0) = 0$. From Eq. (15) it can be seen that for the latter condition to be satisfied the following relation must hold:

$$\frac{\partial n}{\partial \mu} = \frac{4V^2}{z - 4\Gamma_{s+}} \tag{16}$$

in which case, $\Pi(q,\omega)$ takes the form

$$\Pi(q,\omega) = -\frac{\partial n}{\partial \mu}\frac{Dq^2}{Dq^2 + (z - 4\Gamma_{s+})\omega}. \tag{17}$$

When Eq. (16) is combined with the definition of Γ_{0+} as the static limit of the Coulomb interaction, i.e., $\Gamma_{0+} = V^2 \partial \mu/\partial n$, the following expression for Γ_{0+} is obtained: $\Gamma_{0+} = \frac{1}{4}(z - 4\Gamma_s)$. Hence, conservation laws provide the very important relation

$$z = 4(\Gamma_{0+} + \Gamma_{1+}) - \Gamma_{2+} \equiv 4\Gamma_{s+}^{LR}, \tag{18}$$

where $\Gamma_{s+}^{LR} = \Gamma_{1+}^{LR} - \Gamma_{2+}/4$ denotes the singlet amplitude in the presence of long-ranged Coulomb interactions. Since only the Coulomb case is considered in the following, all the Γ_{1+} amplitudes appearing in Eqs. (4a)–(4d), (5), (6a)–(6d), and (7a)–(7d) are to be replaced by their long-ranged counterparts

$$\Gamma_{1+} \to \Gamma_{1+}^{LR} = \Gamma_{0+} + \Gamma_{1+}. \tag{19}$$

Direct inspection of Eqs. (4a)–(4d), (5), (6a)–(6d), and (7a)–(7d) shows that the singlet combination in Eq. (18) is satisfied during the course of renormalization in all the temperature ranges, i.e., $\delta(z - 4\Gamma_s^{LR}) = 0$, provided $\delta\Gamma_{0+} = 0$. (This is a well established result, with great importance for the general structure of the theory.[7,8]) In particular, the corresponding dynamical amplitude $U_{s+}^{LR}(q,\omega)$ reads

$$U_{s+}^{LR}(q,\omega) = \frac{z}{4Dq^2}\frac{1}{\mathcal{D}(q,\omega)}. \tag{20}$$

Note that unlike the U_{s+} amplitude in Eq. (13), U_{s+}^{LR} is a universal amplitude independent of Γ_{s+}^{LR}. This is a direct consequence of singlet relation (18).[6,7]

The scaling equations discussed below are obtained from Eqs. (4a)–(4d), (5), (6a)–(6d), and (7a)–(7d) after (i) rearranging all the $\Gamma_{1\pm}$ amplitudes to give $\Gamma_{s\pm}$ and then replacing Γ_{s+} with Γ_{s+}^{LR}, (ii) replacing the static amplitudes where applicable by the corresponding dynamical amplitudes, and (iii) substituting $\rho = 1/4(2\pi^2 \nu D)$.

It is convenient to express the equation for ρ in terms of the scaling variables, $\gamma_2 = \Gamma_2/z$ and $\gamma_v = -4\Gamma_{s-}/z$. In terms of these variables, the equations for ρ, γ_2, and γ_v form a closed set of equations independent of z. The final RG equations, along with the equations for z, are given below. The scale $\xi = \log(1/T\tau)$ is used in these equations. To logarithmic accuracy $1/\tau$ can be used as the upper cutoff. The range of applicability of ξ is defined in each case separately.

(1) High-temperature limit: $T \gtrsim T_v$ and $T_\perp$,

$$\frac{d\rho}{d\xi} = \rho^2[1 - 15\Phi(\gamma_2)], \tag{21a}$$

$$\frac{d\gamma_2}{d\xi} = \frac{\rho}{2}(1 + \gamma_2)^2, \tag{21b}$$

$$\frac{d\ln z}{d\xi} = -\frac{\rho}{2}(1 - 15\gamma_2). \tag{21c}$$

(2) Low-temperature limit: $T \lesssim T_\perp$,

$$\frac{d\rho}{d\xi} = \rho^2[1 - 3\Phi(\gamma_2)], \tag{22a}$$

$$\frac{d\gamma_2}{d\xi} = \frac{\rho}{2}(1 + \gamma_2)^2, \tag{22b}$$

$$\frac{d\ln z}{d\xi} = -\frac{\rho}{2}(1 - 3\gamma_2). \tag{22c}$$

(3) Intermediate temperature limit: $T_\perp \lesssim T \lesssim T_v$,

$$\frac{d\rho}{d\xi} = \rho^2[1 - \Phi(\gamma_v) - 6\Phi(\gamma_2)], \tag{23a}$$

$$\frac{d\gamma_2}{d\xi} = \frac{\rho}{2}[(1 + \gamma_2)^2 + (1 + \gamma_2)(\gamma_2 - \gamma_v)], \tag{23b}$$

$$\frac{d\gamma_v}{d\xi} = \frac{\rho}{2}(1 + \gamma_v)(1 - \gamma_v - 6\gamma_2), \tag{23c}$$

$$\frac{d\ln z}{d\xi} = -\frac{\rho}{2}(1 - \gamma_v - 6\gamma_2). \tag{23d}$$

The variable $\Phi(\gamma)$ is defined as

$$\Phi(\gamma) = \left(1 + \frac{1}{\gamma}\right)\log(1 + \gamma) - 1. \tag{24}$$

The factors 15 and 3 appearing in Eqs. (21) and (22), respectively, correspond to the number of effective triplet modes. In the case of two distinct, degenerate valleys, the 16 spin-valley modes break up into one singlet and 15 "triplet" modes, while in the limit of strong intervalley scattering the two valleys are effectively combined into a single valley leading to three spin-triplet modes.

When the valleys are split, as in Eq. (23), the amplitude γ_v plays a significant role as the temperature is reduced well below T_v. Given that $\gamma_v=(\Gamma_2-4\Gamma_{1-})/z$ and that $\Gamma_{1-}\approx 0$ for $T\gtrsim T_v$, it follows that $\gamma_v\approx\gamma_2$ as T approaches T_v from above. When $T\ll T_v$, the two amplitudes γ_2 and γ_v diverge from each other significantly. For $T\lesssim T_v$, however, it is reasonable to assume that $\gamma_v\approx\gamma_2$. This is relevant if the lower cutoff $T_\perp$ is not much smaller than T_v. In this case, the equation for ρ and γ_2 pertaining to the different temperature ranges can be combined to give $d\rho/d\xi=\rho^2[1-(4K-1)\Phi(\gamma_2)]$, and $d\gamma_2/d\xi=\rho(1+\gamma_2)^2/2$. Here, $K=n_v^2=4$ when the valleys are degenerate and distinct (high temperature), $K=n_v^2=1$ when intervalley scattering is strong (low temperature), and $K=n_v=2$ when the valleys are distinct but split so that each valley contributes independently (intermediate temperature). For direct comparison with experiments, these simplified equations should suffice for most samples.

The situation changes, however, once $T\ll T_v$, but still greater than $T_\perp$. We see that γ_v and γ_2 evolve differently until γ_v reaches the fixed point value of $\gamma_v^*=-1$ at which point $\Phi(-1)=-1$. (This fixed point is relevant only when $T_\perp\approx 0$.) The system at this point reduces to a single valley system with resistance 2ρ. The above properties are generic to systems with split bands (spin and valley) as has been discussed in detail in Ref. 11.

To summarize, RG equations have been obtained in the case when both valley splitting and intervalley scattering are present. The results can be directly used to compare with experiments in a two-valley system after adding the weak-localization contributions, which are not included here. The case when the two bands are split but otherwise distinct is quantitatively different due to the existence of a third relevant scaling parameter. The asymptotic metallic behavior is, however, not affected.

ACKNOWLEDGMENTS

The author would like to thank A. M. Finkel'stein for numerous discussions on this topic. This work was supported by DOE Grant No. DOE-FG02-84-ER45153 and U.S.-Israel Binational Science Foundation Grant No. 2006375.

APPENDIX A: DIFFUSION PROPAGATORS

The ladder diagrams for each of the diffuson blocks, $\mathcal{D}_{\parallel,u}$, $\mathcal{D}_{\parallel,v}$, and $\mathcal{D}_{\perp,\tau_z}$, are detailed in Fig. 8. The corresponding equations are given in Eq. (A1). Note that the $\mathcal{D}_\parallel$ diffusons are coupled in the presence of intervalley scattering. For convenience, the scattering rates in Eq. (1) are defined as $\Delta_\parallel=1/2\pi\nu\tau_\parallel$ and $\Delta_\perp=1/2\pi\nu\tau_\perp$,

$$\mathcal{D}_{\parallel,u}=\Delta_\parallel+\Delta_\parallel X_\parallel\mathcal{D}_{\parallel,u}+\Delta_\perp X_\parallel\mathcal{D}_{\parallel,v}, \tag{A1a}$$

$$\mathcal{D}_{\parallel,v}=\Delta_\perp+\Delta_\parallel X_\parallel\mathcal{D}_{\parallel,v}+\Delta_\perp X_\parallel\mathcal{D}_{\parallel,u}, \tag{A1b}$$

$$\mathcal{D}_{\perp,\tau_z}=\Delta_\parallel+\Delta_\parallel X_{\perp,\tau_z}\mathcal{D}_{\perp,\tau_z}, \tag{A1c}$$

where

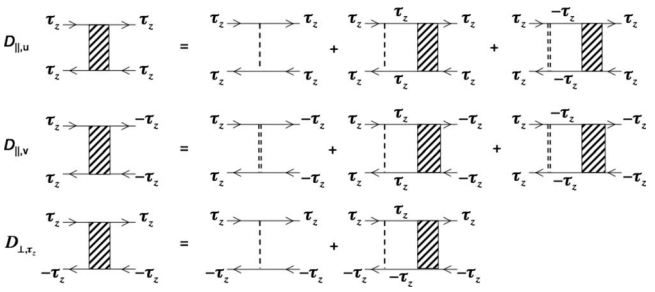

FIG. 8. Ladder diagrams for the various diffuson blocks are shown above. As in Fig. 1, the intravalley and intervalley impurity scatterings are denoted by single and double dashed lines, respectively. The particle and hole Green's functions for finite Δ_v correspond to $\mathcal{G}_{\tau_z}(k,\epsilon)=[i\epsilon-(\xi_k-\tau_z\Delta_v/2)+i/2\tau\,\mathrm{sgn}\,\epsilon]^{-1}$.

$$X_\parallel(q,\omega)=\sum_{\mathbf{k}}\mathcal{G}_{\tau_z}(\mathbf{k}+\mathbf{q},\epsilon+\omega)\mathcal{G}_{\tau_z}(\mathbf{k},\epsilon)$$
$$\approx 2\pi\nu\tau[1-\tau\omega-\tau D_0q^2+\cdots], \tag{A2a}$$

$$X_{\perp,\tau_z}(q,\omega)=\sum_{\mathbf{k}}\mathcal{G}_{\tau_z}(\mathbf{k}+\mathbf{q},\epsilon+\omega)\mathcal{G}_{-\tau_z}(\mathbf{k},\epsilon)$$
$$\approx 2\pi\nu\tau[1-\tau\omega-\tau D_0q^2+i\tau_z(\Delta_v\tau)]. \tag{A2b}$$

Here D is the diffusion constant. In the diffusion approximation, i.e., for $\epsilon(\epsilon+\omega)<0$, it is sufficient to evaluate X in the long wavelength and small frequency limit. Only the weak splitting $\Delta_v\tau\lesssim 1$ limit is considered here.

Equations (A1a) and (A1b) are easily decoupled by defining

$$\mathcal{D}_\pm=\mathcal{D}_{\parallel,u}\pm\mathcal{D}_{\parallel,v}=\frac{1}{2\pi\nu\tau^2}\frac{1}{D_0q^2+\omega+\Delta_\pm}, \tag{A3}$$

where $\Delta_+=0$ and $\Delta_-=2\tau_\parallel/\tau(\tau_\perp-\tau_\parallel)$. Note that $\mathcal{D}_+$ is gapless. Substituting Eq. (A2b) in Eq. (A1c) gives for $\mathcal{D}_{\perp,\tau_z}$

$$\mathcal{D}_{\perp,\tau_z}=\frac{1}{2\pi\nu\tau^2}\frac{1}{D_0q^2+\omega-i\tau_z\Delta_v+\Delta_\perp}, \tag{A4}$$

where $\Delta_\perp=\tau_\parallel/\tau\tau_\perp$.

APPENDIX B: DIFFUSION CORRECTIONS

The expressions for δD and δz extracted from the diagrams in Fig. 4 for the $\mathcal{D}_+$ propagator are given below:

$$\frac{\delta D}{D}=-\frac{4}{\nu}\int\int Dq^2[\mathcal{D}_+^3(q,\omega)(\Gamma_{1+}-\Gamma_{2+})$$
$$+\mathcal{D}_-^3(q,\omega)(\Gamma_{1-}-\Gamma_{2-})+\mathcal{D}_\perp^3(q,\omega)(\Gamma_{1\perp}-2\Gamma_{2\perp})], \tag{B1a}$$

$$\delta z = -\frac{1}{\pi\nu}\int \frac{d^2q}{(2\pi)^2}[\mathcal{D}_+(q,0)(\Gamma_{1+}-\Gamma_{2+}) + \mathcal{D}_-(q,0)(\Gamma_{1-}-\Gamma_{2-}) + \mathcal{D}_\perp(q,0)(\Gamma_{1\perp}-2\Gamma_{2\perp})]. \tag{B1b}$$

(Note the factor of 2 in front of $\Gamma_{2\perp}$; for convenience the τ_z index is suppressed in the $\perp$ terms.) The diffusion corrections to the amplitudes $\Gamma_{i,\alpha}$, where $i=1,2$ and $\alpha=\pm$, are detailed below:

$$\begin{aligned}\delta\Gamma_{1+} = {} & \frac{1}{4\pi\nu}\int \frac{d^2q}{(2\pi)^2}[\Gamma_{2+}\mathcal{D}_+ + \Gamma_{2-}\mathcal{D}_- + 2\Gamma_{2\perp}\mathcal{D}_\perp] \\ & + \frac{1}{\nu}\int\int \Gamma_{2+}[\Gamma_{2+}\mathcal{D}_+^2 + \Gamma_{2-}\mathcal{D}_-^2 + 2\Gamma_{2\perp}\mathcal{D}_\perp^2] \\ & - \frac{1}{2}[\Gamma_{2+}^2\mathcal{D}_+^2 + \Gamma_{2-}^2\mathcal{D}_-^2 + 2\Gamma_{2\perp}^2\mathcal{D}_\perp^2] \\ & - \frac{1}{\nu}\int\int \omega\Gamma_{2+}[\Gamma_{2+}^2\mathcal{D}_+^3 + \Gamma_{2-}^2\mathcal{D}_-^3 + 2\Gamma_{2\perp}^2\mathcal{D}_\perp^3] \\ & - \omega\Gamma_{2+}^2[\Gamma_{2+}\mathcal{D}_+^3 + \Gamma_{2-}\mathcal{D}_-^3 + 2\Gamma_{2\perp}\mathcal{D}_\perp^3] \\ & - \frac{1}{2\nu}\int\int \omega^2\Gamma_{2+}^2[\Gamma_{2+}^2\mathcal{D}_+^4 + \Gamma_{2-}^2\mathcal{D}_-^4 + 2\Gamma_{2\perp}^2\mathcal{D}_\perp^4],\end{aligned} \tag{B2a}$$

$$\begin{aligned}\delta\Gamma_{2+} = {} & \frac{1}{\pi\nu}\int \frac{d^2q}{(2\pi)^2}[\Gamma_{1+}\mathcal{D}_+ + \Gamma_{1-}\mathcal{D}_- + \Gamma_{1\perp}\mathcal{D}_\perp] \\ & + \frac{4}{\nu}\int\int \Gamma_{2+}[\Gamma_{2+}\mathcal{D}_+^2 + \Gamma_{2-}\mathcal{D}_-^2 + 2\Gamma_{2\perp}\mathcal{D}_\perp^2] \\ & - \frac{1}{2}[\Gamma_{2+}^2\mathcal{D}_+^2 + \Gamma_{2-}^2\mathcal{D}_-^2 + 2\Gamma_{2\perp}^2\mathcal{D}_\perp^2] \\ & - \frac{4}{\nu}\int\int \omega\Gamma_{2+}[\Gamma_{2+}^2\mathcal{D}_+^3 + \Gamma_{2-}^2\mathcal{D}_-^3 + 2\Gamma_{2\perp}^2\mathcal{D}_\perp^3] \\ & - \omega\Gamma_{2+}^2[\Gamma_{2+}\mathcal{D}_+^3 + \Gamma_{2-}\mathcal{D}_-^3 + 2\Gamma_{2\perp}\mathcal{D}_\perp^3] \\ & - \frac{2}{\nu}\int\int \omega^2\Gamma_{2+}^2[\Gamma_{2+}^2\mathcal{D}_+^4 + \Gamma_{2-}^2\mathcal{D}_-^4 + 2\Gamma_{2\perp}^2\mathcal{D}_\perp^4],\end{aligned} \tag{B2b}$$

$$\begin{aligned}\delta\Gamma_{1-} = {} & \frac{1}{4\pi\nu}\int \frac{d^2q}{(2\pi)^2}[\Gamma_{2+}\mathcal{D}_- + \Gamma_{2-}\mathcal{D}_+ - 2\Gamma_{2\perp}\mathcal{D}_\perp] \\ & + \frac{1}{\nu}\int\int \Gamma_{2-}[(\Gamma_{2+}+\Gamma_{2-})\mathcal{D}_+\mathcal{D}_- - 2\Gamma_{2\perp}\mathcal{D}_\perp^2] \\ & - \frac{1}{2}[\Gamma_{2-}\Gamma_{2+}(\mathcal{D}_+^2+\mathcal{D}_-^2) - 2\Gamma_{2\perp}^2\mathcal{D}_\perp^2] \\ & + \frac{4}{\nu}\int\int \Gamma_{1-}[(\Gamma_{1+}-\Gamma_{2+})(\mathcal{D}_+\mathcal{D}_- - \mathcal{D}_+^2) \\ & + (\Gamma_{1-}-\Gamma_{2-})(\mathcal{D}_+\mathcal{D}_- - \mathcal{D}_-^2) - 2(\Gamma_{1\perp}-2\Gamma_{2\perp})\mathcal{D}_\perp^2] \\ & - \frac{1}{\nu}\int\int \omega\Gamma_{2-}[\Gamma_{2-}\Gamma_{2+}(\mathcal{D}_-^2\mathcal{D}_+ + \mathcal{D}_-\mathcal{D}_+^2) \\ & - 2\Gamma_{2-}\Gamma_{2\perp}\mathcal{D}_\perp^3] - \omega\Gamma_{2-}^2[\Gamma_{2+}\mathcal{D}_+^2\mathcal{D}_- + \Gamma_{2-}\mathcal{D}_+\mathcal{D}_-^2 \\ & - 2\Gamma_{2\perp}\mathcal{D}_\perp^3] - \frac{1}{\nu}\int\int \omega^2\Gamma_{2-}^2[\Gamma_{2-}\Gamma_{2+}\mathcal{D}_+^2\mathcal{D}_-^2 - \Gamma_{2\perp}^2\mathcal{D}_\perp^4],\end{aligned} \tag{B2c}$$

$$\begin{aligned}\delta\Gamma_{2-} = {} & \frac{1}{\pi\nu}\int \frac{d^2q}{(2\pi)^2}[\Gamma_{1+}\mathcal{D}_- + \Gamma_{1-}\mathcal{D}_+ - \Gamma_{1\perp}\mathcal{D}_\perp] \\ & + \frac{4}{\nu}\int\int \Gamma_{2-}[\Gamma_{2+}\mathcal{D}_+^2 + \Gamma_{2-}\mathcal{D}_-^2 + 2\Gamma_{2\perp}\mathcal{D}_\perp^2] \\ & - \frac{1}{2}[\Gamma_{2-}\Gamma_{2+}\mathcal{D}_+^2 + \Gamma_{2-}^2\mathcal{D}_-^2 + 2\Gamma_{2\perp}^2\mathcal{D}_\perp^2] \\ & + \frac{4}{\nu}\int\int \Gamma_{2-}[\Gamma_{1+}(\mathcal{D}_+\mathcal{D}_- - \mathcal{D}_+^2) + \Gamma_{1-}(\mathcal{D}_+\mathcal{D}_- - \mathcal{D}_-^2) \\ & - 2\Gamma_{1\perp}\mathcal{D}_\perp^2] - \frac{4}{\nu}\int\int \omega\Gamma_{2-}[\Gamma_{2+}^2\mathcal{D}_+^3 + \Gamma_{2-}^2\mathcal{D}_-^3 \\ & + 2\Gamma_{2\perp}^2\mathcal{D}_\perp^3] - \omega\Gamma_{2-}\Gamma_{2+}[\Gamma_{2+}\mathcal{D}_+^3 + \Gamma_{2-}\mathcal{D}_-^3 + 2\Gamma_{2\perp}\mathcal{D}_\perp^3] \\ & - \frac{2}{\nu}\int\int \omega^2\Gamma_{2-}\Gamma_{2+}[\Gamma_{2+}^2\mathcal{D}_+^4 + \Gamma_{2-}^2\mathcal{D}_-^4 + 2\Gamma_{2\perp}^2\mathcal{D}_\perp^4].\end{aligned} \tag{B2d}$$

The terms above are ordered in correspondence with the diagrams appearing in Fig. 5. The square brackets gather vertices that come together with the diffuson propagators. Note that the first term is unique in that it does not involve frequency integration. [If these equations are calculated using perturbation theory, an additional wave-function renormalization term ζ appears.[9] The renormalized amplitudes given below correspond to $\Gamma\zeta^2$, with $\delta\zeta=-\frac{2}{\nu}\int\int(\Gamma_{1+}-\Gamma_{2+})\mathcal{D}_+^2+(\Gamma_{1-}-\Gamma_{2-})\mathcal{D}_-^2+(\Gamma_{1\perp}-2\Gamma_{2\perp})\mathcal{D}_\perp^2$. It should be noted that the term ζ does not appear in the nonlinear sigma model approach developed in Ref. 7.]

*punnoose@sci.ccny.cuny.edu

[1] A. Punnoose and A. M. Finkel'stein, Phys. Rev. Lett. **88**, 016802 (2001).
[2] A. Punnoose and A. M. Finkel'stein, Science **310**, 289 (2005).
[3] S. Anissimova, S. V. Kravchenko, A. Punnoose, A. M. Finkel'stein, and T. M. Klapwijk, Nat. Phys. **3**, 707 (2007).
[4] D. A. Knyazev, O. E. Omel'yanovskii, V. M. Pudalov, and I. S. Burmistrov, JETP Lett. **84**, 662 (2007).
[5] D. A. Knyazev, O. E. Omel'yanovskii, V. M. Pudalov, and I. S. Burmistrov, Phys. Rev. Lett. **100**, 046405 (2008).
[6] B. L. Altshuler and A. G. Aronov, *Modern Problems in Condensed Matter Physics* (Elsevier/North-Holland, New York/Amsterdam, 1985), p. 1.
[7] A. M. Finkel'stein, Sov. Phys. JETP **57**, 97 (1983).
[8] A. M. Finkel'stein, Sov. Sci. Rev., Sect. C, Math. Phys. Rev. **14**, 1 (1990).
[9] C. Castellani, C. Di Castro, P. A. Lee, and M. Ma, Phys. Rev. B **30**, 527 (1984).
[10] T. Ando, A. B. Fowler, and F. Stern, Rev. Mod. Phys. **54**, 437 (1982).
[11] I. S. Burmistrov and N. M. Chtchelkatchev, Phys. Rev. B **77**, 195319 (2008).
[12] S. V. Kravchenko, G. V. Kravchenko, J. E. Furneaux, V. M. Pudalov, and M. D'Iorio, Phys. Rev. B **50**, 8039 (1994).
[13] M. Rahimi, S. Anissimova, M. R. Sakr, S. V. Kravchenko, and T. M. Klapwijk, Phys. Rev. Lett. **91**, 116402 (2003).
[14] H. Fukuyama, J. Phys. Soc. Jpn. **49**, 649 (1980).
[15] H. Fukuyama, J. Phys. Soc. Jpn. **50**, 3562 (1981).
[16] Ando Tsuneya, Surf. Sci. **98**, 327 (1980).
[17] P. A. Lee and T. V. Ramakrishnan, Phys. Rev. B **26**, 4009 (1982).
[18] B. L. Altshuler, A. G. Aronov, and P. A. Lee, Phys. Rev. Lett. **44**, 1288 (1980).
[19] A. M. Finkel'stein, Z. Phys. B **56**, 189 (1984).